OPTIMAL CONTROL APPLICATIONS AND METHODS
Optim. Control Appl. Meth. (2013)
Published online in Wiley Online Library (wileyonlinelibrary.com). DOI: 10.1002/oca.2099

Human-inspired motion primitives and transitions for bipedal robotic locomotion in diverse terrain

H. Zhao*,†, M. J. Powell and A. D. Ames

Department of Mechanical Engineering, Texas A&M University, College Station, TX 77843, USA

SUMMARY

In this paper, a control design approach is presented, which uses human data in the development of bipedal robotic control techniques for multiple locomotion behaviors. Insight into the fundamental behaviors of human locomotion is obtained through the examination of experimental human data for walking on flat ground, upstairs, and downstairs. Specifically, it is shown that certain outputs of the human, independent of locomotion terrain, can be characterized by a single function, termed the *extended canonical human function*. Through feedback linearization, human-inspired locomotion controllers are leveraged to drive the outputs of the simulated robot, via the extended canonical human function, to the outputs from human locomotion. An optimization problem, subject to the constraints of *partial hybrid zero dynamics*, is presented that yields parameters of these controllers that provide the best fit to human data while ensuring stability of the controlled bipedal robot. The resulting behaviors are stable walking on flat ground, upstairs, and downstairs—these three locomotion modes are termed 'motion primitives'. A second optimization is presented, which yields controllers that evolve the robot from one motion primitive to another—these modes of locomotion are termed 'motion transitions'. A directed graph consisting these motion primitives and motion transitions has been constructed for the stable motion planning of bipedal locomotion. A final simulation is given, which shows the controlled evolution of a robotic biped as it transitions through each mode of locomotion over a pyramidal staircase.

Received 4 January 2012; Revised 6 September 2013; Accepted 9 October 2013

KEY WORDS: hybrid robotic systems; human-inspired optimal control; stair climbing; motion planning

1. INTRODUCTION

Obtaining truly human-like bipedal robotic walking has been one of the most prominent goals of the humanoid robotics community. The need for functional robots, and the understanding thereof, is apparent in many fields today. In light of recent events, such as the tragic crisis at the Fukushima nuclear plant in Japan, robots are needed that can traverse dangerous terrain and work in virulent environments [1, 2]. Robots capable of human-like walking, climbing, running, and all the basic modes of human locomotion are necessary for truly successful cooperation with mankind. Moreover, achieving human-like bipedal robotic locomotion can inversely help humans understand the human body in more depth. This understanding can be leveraged to build prosthetic devices [3–5] for lower extremity amputees, which will help them walk with a gait as natural as a healthy human. Therefore, the important and far-reaching ramifications of obtaining human-like bipedal walking have attracted many researchers from a variety of fields of study.

During three decades of study, researchers have accomplished a remarkable number of achievements on bipedal walking and climbing. Honda's ASIMO [6] has been the most popular humanoid robot around the world, yet its fundamental control scheme is to keep the center of pressure within

*Correspondence to: H. Zhao, Department of Mechanical Engineering, Texas A&M University, College Station, TX 77843, USA.
†E-mail: huihuazhao@tamu.edu

the support polygon all the time (which is known as the ZMP (Zero Moment Point) method). Attracted by the energy efficiency and the human-like aesthetics of passive walking [7], which was first realized by Tad McGeer, a number of robots, such as [8, 9], Flame of TU Delft, have been constructed using this basic principle. Jessy Grizzle's planar robot MABEL [10] holds the title of the quickest bipedal robot in the world—and can also walk on uneven terrains. Most of the current research in bipedal robotics is focused on 2D locomotion, that is, planar robots.

Taking a different approach, we leverage the knowledge of human body to develop locomotion control schemes. The quintessential model of bipedal locomotion—the human body—is the most prevalent source of information on bipedal walking. The physical human system, which utilizes 57 muscles in locomotion [11], is far too complex to replicate with current hardware and computational capabilities. However, one can construct a low-level representation of the human locomotion system. That is, from a control theorist perspective, one can view the human body as a 'black box', while certain outputs of which can be represented by simple, time-based functions. Utilizing these outputs functions via the feedback linearization control method, the robot will display the same qualitative behavior as the human, despite the physical differences between the two systems. This approach is similar to the work of others in the control and biomechanical fields. By merging human data and hybrid zero dynamics, Westervelt [12] has achieved stable walking for a five-link robot model in simulation with Bezier series fit to the human data. A work based on the same fitting method can also be found in [13]. Predictive dynamics with B-spline fit to human data has been applied to simulate normal human walking and human walking with external load [14]. Polynomial function is also one of the popular choices used to characterize outputs of human [15, 16]. However, unlike all these functions, the method proposed in this work offers a simpler formula that can represent all the motion primitives and motion transitions with high correlations while rendering more robustness outside the operation region.

In this paper, a human-inspired controller is considered that utilizes the simple low dimensional function—*extended canonical human function* (ECHF)—to represent human walking. The study begins with examination of the human locomotion system. Three experiments are performed, which yield human xyz-position data for flat-ground walking, walking upstairs, and walking downstairs; these data form the foundation of our control approach. Specifically, the ECHF is shown to represent the sets of data, from three modes of locomotion (walking on flat ground, upstairs, and downstairs) of interest and four transition modes, with high correlation in each case. More importantly, it is found that the ECHF tends to have a more stable behavior even outside the operation region while other methods are easy to blow up if considered outside the operation window. This is very important especially for a physical robot that is vulnerable to the various environment uncertainty and disturbance. We have successfully achieved the physical bipedal robotic walking on flat ground, upslope, and rough terrain of AMBER with the proposed ECHF [17] (Texas A&M University, College Station, Texas, USA). We argue that it is the special form of the function on which the controller is based that plays a key role to the easy implementation (corresponding to the fewer parameters) and the robustness of the walking (corresponding to the better behavior outside the region of definition).

A formal construction scheme for hybrid systems—the *meta-hybrid system*—is presented, in which a distinction is made between primary and auxiliary modes of locomotion, which are termed *motion primitives* and *motion transitions*, respectively. Motion primitives are fundamental modes of locomotion; the four motion primitives of this study are the following: standing still on flat ground, walking on flat ground, upstairs, and downstairs. Because of the differences of modeling, we separate the four motion primitives into two groups: The first group only contains a standing still mode and is termed as 'stationary motion primitive'; the second group includes the remaining three locomotion behaviors and is termed the 'mobile motion primitives'. To switch between different motion primitives in a stable manner, auxiliary modes, termed 'motion transitions', are introduced.

To summarize, this paper presents two main results; the first is an extension of [18], in which the author presents a method of automatically obtaining robotic walking controllers, via an optimization, from a set of human walking data. In this framework, it is shown that an augmentation of the optimization can be successfully applied to multiple modes of locomotion. An extending result of [19] is given in which it is shown that the solution to the optimization problem, which

DOI: 10.1002/oca

minimizes the cost of the least square fits of the control outputs to corresponding human data, ensures *partial hybrid zero dynamics* (PHZD) and thus yields stable walking controllers for walking on flat ground, upstairs and downstairs. Other works related to robotic walking on uneven terrain or staircases can be found in [20–22]; however, none of these contributions consider human-like staircase locomotion. The second result is that by utilizing the same optimization problem, subject to different constraints, we can achieve controllers that evolve the robot from one locomotion mode to another. The combination of these two results is a collection of controllers, automatically obtained from optimizations about human data, which form a continuous, multimodel system.

Compared with the preamble work [23] that has been submitted to the IEEE ICRA 2012, this manuscript provides full development of all the concepts needed for the reader to completely understand this work. Aside from this fact, the journal version stands out with the following improvements: (i) Instead of only using one subject's data, as is performed in the ICRA paper, this manuscript utilizes the mean human data computed from six subjects, which makes our conclusions more general and believable. (ii) In the ICRA paper, we did not consider human data for the transition motions. However, in this manuscript, we consider the human data for the stationary related transition motions. Readers can notice that when considering human data, the transition behaviors are more human-like and yield lower angular velocities and thus lower torques. (iii) Compared with the ICRA paper, we have added standing still and transitions between standing and walking on flat ground. This makes the collection of motion primitives of the robot more realistic.

2. HUMAN LOCOMOTION DATA

The most prevalent source of information on bipedal robotic walking found in nature is the human body. This section provides an overview of the analysis and insight obtained through examination of human walking. Data were collected from three separate experiments in which subjects were instructed to perform different types of locomotion: walking on flat ground, ascending a stairway, and descending a stairway. Single step data are isolated from the experiment data via a procedure termed the domain breakdown for each type of motion of each subject. The *extended canonical function* is proposed and shown to universally represent specific kinematic outputs of the human body for all three motion primitives and four motions transitions considered in this paper.

2.1. Human locomotion experiments

Three experiments, which were performed at different times, were set up for different parts of data. Flat-ground walking data were collected from the first two experiments. Data of ascending and descending a stairway were obtained from the third experiment. A total of 15 human subjects participated in this study; each was outfitted with 19 LED sensors placed at key locations on the body (as illustrated in Figure 1). As a test subject performs the desired task, data were collected from these sensors via the Phase Space Motion Capture System.[‡] During the first and second experiments, test subjects were informed to walk 3 m along a line drawn on the floor. Each subject repeated the same process 12 times per experiment. In the third experiment, the test subjects were instructed to perform two modes of locomotion: ascending a stairway and descending a stairway. The stairway used in this experiment has a 0.152 m stair height and a 0.254 m stair depth. Note that all experiments are carried out by our collaborator motion capture lab in the University of California at Berkeley with the Institutional Review Board protocol #2011 − 04 − 3088.

For each subject, data that contain the least noise were used in the computation of kinematic outputs. Here, the 'noisy' data are mainly from time to time dysfunction of the sensors. An average is computed of all the subjects' data for a given output; this average is termed the 'mean human data' corresponding to the kinematic output. It is the analysis of this mean human data that forms the basis of our locomotion controller design.

[‡]Available from: http://www.phasespace.com/ (2011).

DOI: 10.1002/oca

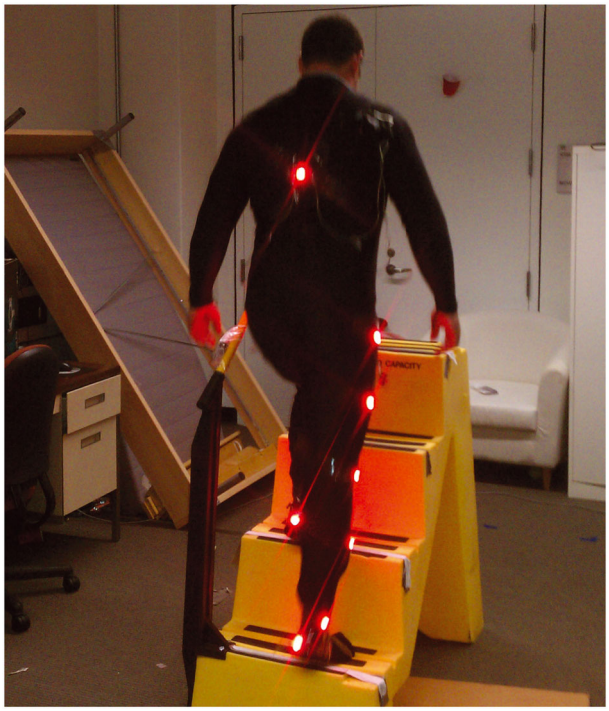

Figure 1. Human experiment for walking upstairs.

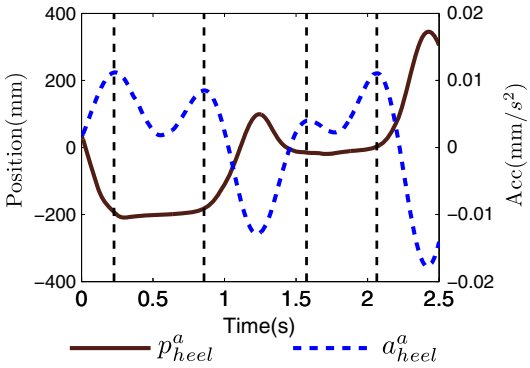

Figure 2. Domain breakdown for walking upstairs.

2.2. *Automated domain breakdown*

The process by which the start and end of a single step are determined is termed the *domain breakdown* procedure. Generally, the domain breakdown is obtained through a position threshold that specifies when the heel or toe is on the ground. However, a new method is proposed here, by utilizing the acceleration data—rather than position—of the heel and toe to determine the single step interval, which is motivated by noting that the time when heel hits or lifts the ground is the moment that maximum acceleration occurs. Data of the position and acceleration of a test subject's heel during the stair ascending are shown in Figure 2. The peak accelerations are indicated with dashed vertical lines. The corresponding positions of the heel show the moment of heel strike and lift.

This method is similar to the analysis of ground reaction forces using force plate, which is common in the biomechanics community [24, 25]. The domain breakdown plays a critical role in the human-inspired locomotion controller design process; that is, the complete-step time intervals obtained through the domain breakdown specify the intervals of data over which our function fitting method is valid, that is, the nominal operation region of our controller.

DOI: 10.1002/oca

2.3. Extended canonical human function

In [26], it is shown that certain kinematic outputs of human walking can be represented by a single, universal function termed the 'canonical human function'—which is the solution to a linear spring-damper system under constant force. Examination of the data for walking upstairs and downstairs, however, reveals a need for the augmentation of this function. It is found that walking upstairs and downstairs, and the transitions between these behaviors and flat-ground walking, can be represented—with a high degree of accuracy—by the response of a linear spring-mass-damper system subject to a sinusoidal excitation, which has the form

$$y = \underbrace{e^{-\xi\omega_n t}(c_0\cos(\omega_d t) + c_1\sin(\omega_d t)) + g_0/\omega_n^2}_{\text{'human'=linear spring-mass-damper system}} + \underbrace{c_2(\omega_n,\omega,\zeta,b)\cos(\omega t) + c_3(\omega_n,\omega,\zeta,b)\sin(\omega t)}_{\text{'environment'=sinusoidal excitation}}, \tag{1}$$

where c_0 and c_1 are the initial conditions decided by the initial position $y(0)$ and the initial velocity $\dot{y}(0)$, ξ is the damping ratio, ω_n is the natural frequency, $\omega_d = \sqrt{1-\xi^2}\omega_n$ is the damped frequency, the constant term g_0 is the gravity term, b and ω are the amplitude and frequency of the sinusoidal excitation, respectively; c_2 and c_3 are functions of ω_n, ω, ξ, and b given by

$$c_2 = (2b\xi\omega)/(\omega^4 + 2(-1+2\xi^2)\omega^2\omega_n^2 + \omega_n^4), \tag{2}$$

$$c_3 = (b(-\omega^2+\omega_n^2))/(\omega^4 + 2(-1+2\xi^2)\omega^2\omega_n^2 + \omega_n^4). \tag{3}$$

Manipulation of (1) yields the following simplified form, which we term the ECHF:

$$y_H(t) = e^{-\alpha_1 t}(\alpha_2\cos(\alpha_3 t) + \alpha_4\sin(\alpha_3 t)) + \alpha_5\cos(\alpha_6 t) + \kappa(\alpha)\sin(\alpha_6 t) + \alpha_7, \tag{4}$$

where $\kappa(\alpha) = (2\alpha_1\alpha_5\alpha_6)/(\alpha_1^2+\alpha_3^2-\alpha_6^2)$. Comparing this form with the solution of linear spring-mass-damper systems, we have $\alpha_1 = \xi\omega_n$, $\alpha_2 = c_1$, $\alpha_3 = \omega_d$, $\alpha_4 = c_1$, $\alpha_5 = c_2$, $\alpha_6 = \omega$, and $\alpha_7 = g_0/\omega_n^2$. Note that in the form of (1), the homogenous solution terms and the gravity related constant correspond to the basic solution of the 'linear spring-mass-damper' system of human locomotion while the sinusoidal excitation terms are due to the external excitation imparted on the system by the environment—which is, in this case, the elevation of the walking surface. Moreover, for the case of walking on flat ground, the sinusoidal excitation terms can be removed, which is the case discussed in [18]. The reason to execute this manipulation (4) is that the ECHF has a simpler form that yields efficiency for the optimization problem that will be discussed later.

With the ECHF in hand, it is important to note how the ideas considered in this paper, and the control approach taken, draw motivation from human walking. The realization of physical human walking is achieved via a highly sophisticated and complex system—the coordination of the muscular and nervous systems required even for the simple task of taking one step is still not fully understood. Therefore, rather than trying to understand the complete dynamics of human walking, we take a control theorist perspective: We view the human walking system as a 'black box'. In this light, the problem becomes to find the 'outputs' of this black box that characterize the behavior of the system. By tracking these outputs in a robot, through virtual output constraints, the result is a robot that displays the same qualitative behaviors as the human despite the differences in dynamics. Similar approaches have been taken in the robotics community; some of these approaches to note are the following: polynomial functions used in [27], B-spline functions in [28], and Bezier series applied in [12, 13]. However, unlike all these functions, the ECHF provides a simpler form (requires fewer parameters) that appears to characterize all the basic human locomotion primitives (walking, stair ascending, stair descending, and running [38]). Moreover, another advantage to our approach over other similar methods (e.g., a $4th$ order polynomial function used in [15]) is the better behavior of the ECHF outside the nominal operation region. As shown in Figure 3, both the ECHF (with correlation as 0.9934) and the $4th$ order polynomial function (with the correlation as 0.9875) can fit the human data very well. However, the $4th$ order polynomial function blows up outside the operation window immediately and becomes infeasible while the ECHF still remains a reasonable value, which we claim is very important to give the robot more robustness while handling the external disturbance. As a robot will always miss the designed right time frame in real world because of the

DOI: 10.1002/oca

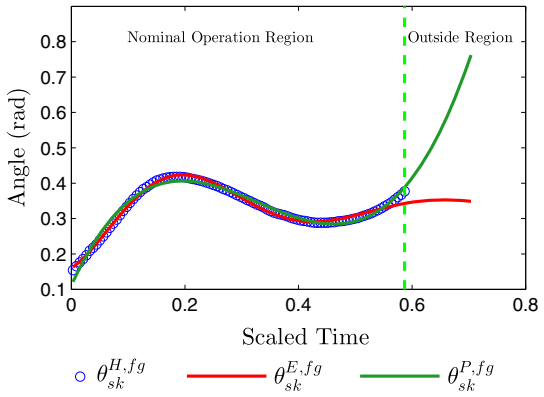

Figure 3. Stance knee angle data fit comparison between the extended canonical human function (ECHF) and the $4th$ order polynomial function outside of the nominal operation region, which is obtained by extending 20% of the nominal operation region. The superscripts H, E, and P denote the human data, ECHF fitting, and polynomial fitting, respectively.

environment disturbance and model uncertainty, the behavior outside the nominal region plays a key role to the stability and robustness of the robot. Evidence of the robustness of using the ECHF on a physical robot can be seen on AMBER [29]. In the next section, we discuss the specific outputs chosen to characterize human walking and show that the ECHF represents these certain outputs of human data with high correlations.

2.4. Human outputs

While analyzing the human data, we seek human outputs that satisfy the specific criteria mentioned in [18]. A total of four kinematic outputs are required for the fully actuated four-DOF robot model in consideration. Analysis of the human data yields the following four outputs (seen in Figure 6(c)), which seem to fully describe the four-DOF analog of the human locomotion system:

1. the linearized forward position of the hip,

$$\delta p_{hip} = -\theta_{sf} L_c + (-\theta_{sf} - \theta_{sk}) L_t,$$

   where L_c and L_t are the lengths of the calf and thigh, respectively, and θ_{sf} is the stance ankle angle measured from the vertical line to the calf, which can be seen in Figure 6(a);
2. the hip angle, θ_{hip}, which is the angle measured from stance thigh to nonstance thigh;
3. the stance knee angle θ_{sk};
4. the nonstance knee angle, θ_{nsk}.

To calculate the mean human outputs, the following three steps are performed. First, we compute the kinematic outputs, from human data, of all six subjects considered in this paper. The mass and length distribution for each subject can be seen in Table I. Second, we determine which subject has the shortest single step interval, via using the domain breakdown procedure from Section 2.2. Then, we denote this step interval as the 'reference step interval'. For all other subjects, we scale all four kinematic outputs to the reference step interval. Finally, we average the outputs of all six subjects to obtain the mean human outputs, which can be seen in Figures 4 and 5. Explicitly, fg, us, and ds correspond to the data of walking on flat ground, upstairs, and downstairs, respectively. And $f \to u$ represents the data of transition from walking on flat ground to walking on upstairs; similar definition holds for other three terms.

Examination of human locomotion data reveals that the time derivative of linearized hip position is approximately constant, as seen in Figures 4(a) and 5(a). Thus, we fit the linearized hip position

DOI: 10.1002/oca

Table I. Description of each of the subjects.

Subject	Age (years)	Height (m)	Weight (kg)	m_h (kg)	m_t (kg)	m_c (kg)	L_t (mm)	L_c (mm)
S_1	30	173	82.5	50.7	7.5	3.5	45.8	38.5
S_2	30	163	69.5	42.7	6.3	3.5	39.0	36.6
S_3	30	160	65.0	40.0	5.9	2.7	36.8	32.7
S_4	26	164	67.5	41.5	6.1	2.8	38.1	36.5
S_5	25	182	92.5	56.9	8.4	3.9	47.1	41.2
S_6	25	166	58.4	35.9	5.3	2.5	40.5	38.0
S_{mean}	27.7	168	72.6	44.1	6.5	3.0	41.0	37.5

The subject number is in the left column, and the L_c (mm), L_t(mm), m_c (kg), and m_t (kg) measurements correspond to the lengths described in Figure 6(a). The measurements m_c and m_t are calculated according to the mass distribution in Ref. [30].

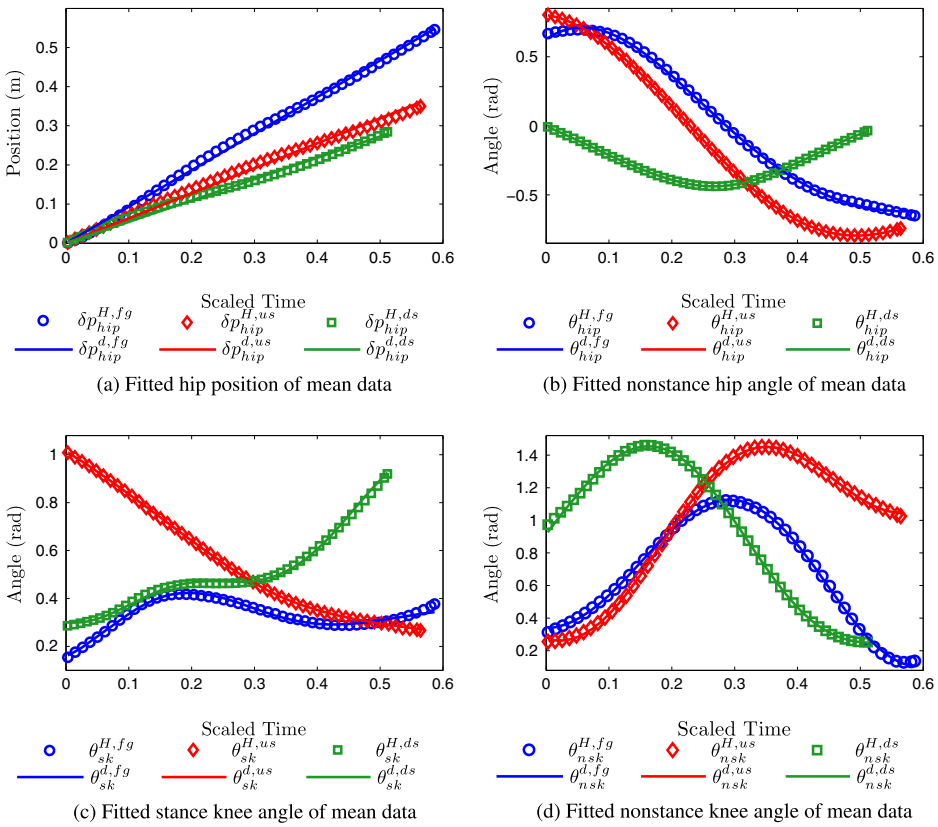

(a) Fitted hip position of mean data

(b) Fitted nonstance hip angle of mean data

(c) Fitted stance knee angle of mean data

(d) Fitted nonstance knee angle of mean data

Figure 4. Fitted extended canonical human function and corresponding mean human data of motion primitives.

with straight line as $\delta p_{hip}^{d} = v_{hip} t$, where v_{hip} is the forward hip velocity. Utilizing the ECHF, the remaining three desired outputs of a robot can be stated as follows:

$$\begin{aligned} \theta_{hip}^{d}(t, \alpha_{hip}) &= y_H(t, \alpha_{hip}), \\ \theta_{sk}^{d}(t, \alpha_{sk}) &= y_H(t, \alpha_{sk}), \\ \theta_{nsk}^{d}(t, \alpha_{nsk}) &= y_H(t, \alpha_{nsk}), \end{aligned} \tag{5}$$

where, for example, $\alpha_{sk} = (\alpha_{sk,1}, \alpha_{sk,2}, \alpha_{sk,3}, \alpha_{sk,4}, \alpha_{sk,5}, \alpha_{sk,6}, \alpha_{sk,7})$ in (4). The parameters of all the outputs can be combined into a single parameter vector: $\alpha = (v_{hip}, \alpha_{hip}, \alpha_{sk}, \alpha_{nsk}) \in \mathbb{R}^{22}$. By

DOI: 10.1002/oca

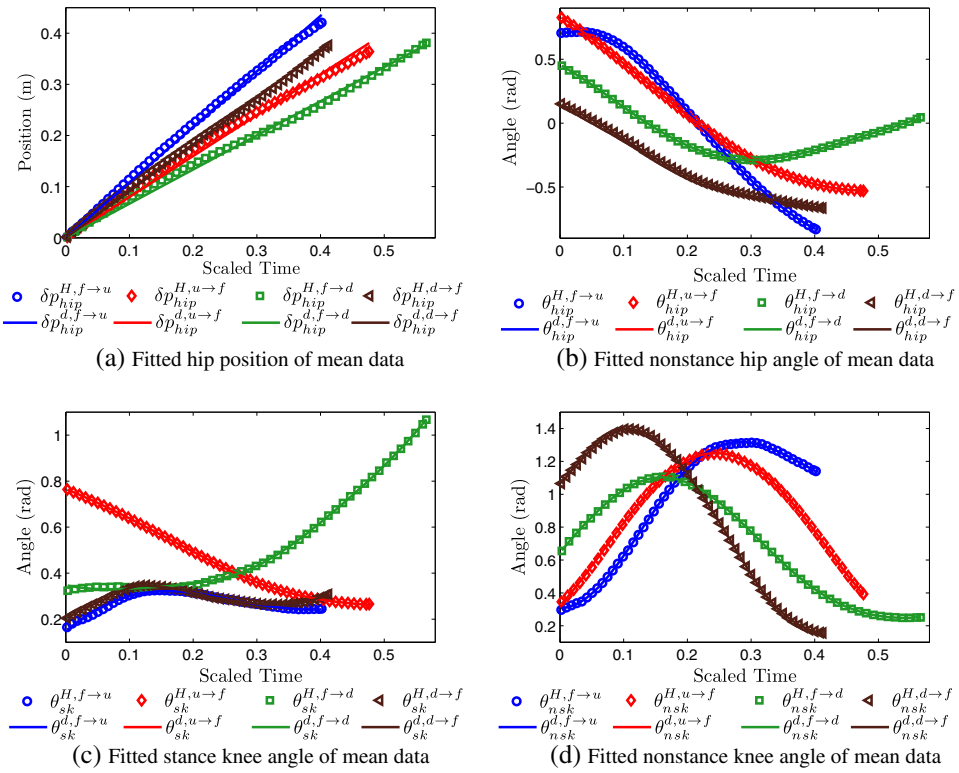

(a) Fitted hip position of mean data

(b) Fitted nonstance hip angle of mean data

(c) Fitted stance knee angle of mean data

(d) Fitted nonstance knee angle of mean data

Figure 5. Fitted extended canonical human function and corresponding mean human data of motion transitions.

fitting these functions, via least square fits that yield high correlation coefficients, to corresponding human data, we claim that the canonical human function accurately describes human walking data.

To determine the parameters for the ECHF, the following optimization is solved:

$$\alpha^* = \underset{\alpha \in \mathbb{R}^{22}}{\operatorname{argmin}} \ \mathrm{Cost}_{\mathrm{HD}}(\alpha). \tag{6}$$

This optimization problem produces the least square fits (the detailed form of the cost function can be referred to [18]) of the ECHF to the corresponding human data. The parameters obtained through this process are given in Table II, together with the correlation of each function to the corresponding set of data. Additionally, the functions for each kinematic constraint and each locomotion behavior (three motion primitives and four motion transitions) are plotted with the corresponding human data in Figures 4 and 5. Note that all the correlations are higher than 0.99, which implies that the ECHF can be fitted to the outputs of all three types of motion primitive and four types of motion transition universally with a high degree of accuracy.

3. ROBOT MODEL

With the goal to achieve human-like robotic walking, we consider a robotic model with mass and length parameters as determined by human subject data. To reduce computational complexity, while preserving the form of the human lower body, we construct the model as a serial chain of rigid links. Each link l has a length L_l and a mass m_l, which is a point mass located at a distance r_l from the base of the link. The resulting model configuration is shown in Figure 6(a), while the mass and length distribution are shown in Figure 6(b). The specific values of these parameters for each single subject are obtained by applying Winter's [30] mass and length distribution to the human test subject. The mass and length of all subjects considered in this paper are averaged to obtain the parameters of the mean human data model, which can be seen in Table II. The modeling process

DOI: 10.1002/oca

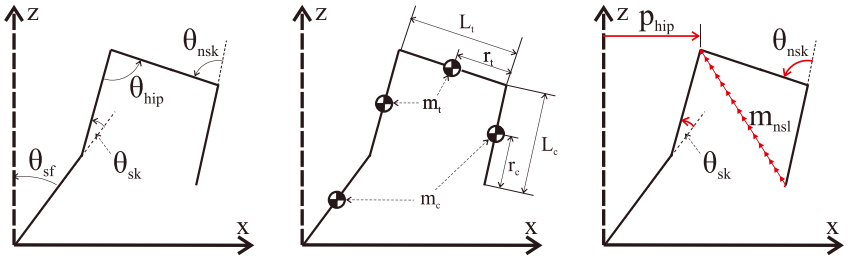

(a) Robot configuration. (b) Robot mass-length. (c) Robot outputs.

Figure 6. The modeled robot's configuration, mass and length distribution, and virtual constraints.

Table II. Fitted parameter values for human functions.

	$y_1^d = a_1 t, \quad y_2^d = y_H(t)$ given in (4)							
Function	a_1	a_2	a_3	a_4	a_5	a_6	a_7	Correlation
δp_{hip}^{fg}	0.934	0	0	0	0	0	0	0.9991
δp_{hip}^{us}	0.639	0	0	0	0	0	0	0.9954
δp_{hip}^{ds}	0.546	0	0	0	0	0	0	0.9976
θ_{hip}^{fg}	2.675	0.981	6.063	0.937	0	0	−0.353	0.9991
θ_{hip}^{us}	2.093	1.192	6.039	0.286	−0.038	12.572	−0.353	1.0000
θ_{hip}^{ds}	0.103	0.158	8.167	−0.238	−0.009	22.08	−0.153	0.9999
θ_{sk}^{fg}	3.322	−0.174	13.66	0.040	0	0	0.333	0.9934
θ_{sk}^{us}	4.402	0.787	3.318	0.543	−0.010	16.09	0.236	1.0000
θ_{sk}^{ds}	0.548	−10.34	0.535	−11.35	−0.065	17.33	10.70	0.9992
θ_{nsk}^{fg}	−0.861	−0.344	10.57	0.046	0	0	0.681	0.9996
θ_{nsk}^{us}	−2.059	0.276	0.074	1.072	−0.409	10.90	0.407	0.9999
θ_{nsk}^{ds}	2.667	1.264	3.460	2.197	−0.180	13.90	−0.172	0.9998
$\delta p_{hip}^{f\to u}$	1.085	0	0	0	0	0	0	0.9993
$\delta p_{hip}^{u\to f}$	0.799	0	0	0	0	0	0	0.9981
$\delta p_{hip}^{f\to d}$	0.668	0	0	0	0	0	0	0.9990
$\delta p_{hip}^{d\to f}$	0.913	0	0	0	0	0	0	0.9996
$\theta_{hip}^{f\to u}$	−3.215	0.331	7.876	−0.045	0.087	16.66	0.276	1.0000
$\theta_{hip}^{u\to f}$	0.444	0.186	1.747	−1.741	0.160	8.610	0.490	1.0000
$\theta_{hip}^{f\to d}$	−0.227	−0.102	4.192	−0.697	0.064	13.58	0.495	1.0000
$\theta_{hip}^{d\to f}$	−2.480	−0.947	1.930	0.041	0.044	16.87	1.050	0.9999
$\theta_{sk}^{f\to u}$	0.705	−0.191	9.239	0.872	0.140	9.420	0.200	0.9940
$\theta_{sk}^{u\to f}$	3.820	0.514	4.154	0.185	−0.009	17.24	0.261	1.0000
$\theta_{sk}^{f\to d}$	−1.307	−0.556	2.804	0.069	−0.010	22.05	0.914	0.9997
$\theta_{sk}^{d\to f}$	1.057	−0.703	5.593	1.094	0.611	6.759	0.278	0.9901
$\theta_{nsk}^{f\to u}$	0.217	−0.473	9.417	−0.021	−0.128	15.81	0.908	0.9999
$\theta_{nsk}^{u\to f}$	1.691	−0.335	7.973	−0.265	−0.019	8.197	0.677	0.9999
$\theta_{nsk}^{f\to d}$	0.919	0.112	8.101	0.574	−0.034	16.88	0.567	1.0000
$\theta_{nsk}^{d\to f}$	1.301	0.372	10.82	−0.024	−0.106	11.14	0.777	0.9999

considers the common assumptions in the bipedal robot literature [10], which imply the existence of both continuous and discrete dynamic behaviors that are observed in phases of single support and double support. Based on the model specifications, the following sections give the derivation of the dynamics of the system.

DOI: 10.1002/oca

3.1. Continuous dynamics

Given the configuration space $\mathcal{Q}$: $q = \{\theta_{sf}; \theta_{sk}; \theta_{hip}; \theta_{nsk}\}$, using the method of Lagrange with holonomic constraints, we can obtain the dynamics of the continuous phase as

$$D(q)\ddot{q} + H(q,\dot{q}) + A^T(q)\lambda = B(q)u, \tag{7}$$

where $D(q)$ and $B(q)$ are the generalized inertia and torque distribution maps, respectively, and $H(q,\dot{q}) = C(q,\dot{q})\dot{q} + G(q)$ contains terms resulting from the Coriolis effect and gravity. Note that, here, $B(q)u$ provides full actuation as modeled, which will be discussed later in Section 4. $A(q) \in \mathbb{R}^{k\times n}$ is a set of k velocity constraints corresponding to holonomic constraints; λ are Lagrange multipliers that are used to enforce holonomic constraints. The formula of λ can be given with the method from Chapter 6 in [31] as follows:

$$\lambda = (A(q)D(q)^{-1}A(q)^T)^{-1}(\dot{A}(q)\dot{q} + A(q)D^{-1}(B(q)u - H(q,\dot{q}))). \tag{8}$$

Substituting this equation back into (7) leads to the affine control system for the continuous dynamics, FG:

$$\dot{x} = f(q,\dot{q}) + g(q)u, \tag{9}$$

where $f(q,\dot{q})$ and $g(q)$ are defined as follows:

$$f(q,\dot{q}) = \begin{bmatrix} \dot{q} \\ D^{-1}(q)(A^T(q)\Theta(q)A(q)D^{-1}(q) - I) \\ (H(q,\dot{q}) - A^T(q)\Theta(q)\dot{A}(q)\dot{q}) \end{bmatrix}, g(q) = \begin{bmatrix} \mathbf{0} \\ D^{-1}(q)(I - A^T(q)\Theta(q)A(q))B(q) \end{bmatrix}, \tag{10}$$

where, for simplicity, $\Theta(q) = A(q)D^{-1}(q)A^T(q)$.

In this paper, two types of continuous walking behavior with different dynamic models are considered. The first type is stationary behavior that contains standing still on flat ground, in which case both feet are pinned to the ground. The second type is a set of three mobile behaviors, in which case one leg is pinned to the ground while the other leg swings freely.

3.1.1. Stationary motion primitive. For stationary behavior, Lagrange multipliers are needed to ensure that the swing foot remains in contact with the ground. Thus, $f_s(q,\dot{q})$ and $g_s(q)$ are defined with the form given by (10).

3.1.2. Mobile motion primitive. For the mobile behavior, the swing foot is not constrained, that is, $A(q) = 0$. Thus, the affine control system of mobile locomotion can be reduced to the following form:

$$f_m(q,\dot{q}) = \begin{bmatrix} \dot{q} \\ D^{-1}(q)H(q,\dot{q}) \end{bmatrix}, \quad g_m(q) = \begin{bmatrix} \mathbf{0} \\ D^{-1}(q)B(q) \end{bmatrix}. \tag{11}$$

3.2. Discrete dynamics

With the modeling assumption that the discrete dynamics phase occurs instantaneously, the dynamic response is modeled as an impact on the system. Specifically, the method of [32] is used to model the plastic rigid-body impacts as impulse responses. The detailed derivation can be found in Chapter 3 in [10]; thus, it is omitted here for space consideration.

With the assumption of symmetric walking, we use a stance/nonstance notation for the legs. To effect this statement that the legs be 'switched' at impact, and thereby reduce the complexity of the model, the reset map can be implemented as follows:

$$\Delta(q,\dot{q}) = \begin{bmatrix} \Delta_q q \\ \Delta_{\dot{q}}(q)\dot{q} \end{bmatrix}, \tag{12}$$

where Δ_q is the relabeling [18, 33] that switches the stance and nonstance leg at impact, and $\Delta_{\dot{q}}$ determines the change of velocity due to the impact. Further details can be found in [18].

DOI: 10.1002/oca

4. CONTROLLER DESIGN

The purpose of this section is to specify a controller, u, for the given control system (10). Motivated by the desire to obtain human-like bipedal robotic locomotion, we seek to construct a controller that drives the outputs of the robot to the corresponding outputs of the human. Formally, we seek a u_α that guarantees that $y^a(q) \to y^d_\alpha(t)$ as $t \to \infty$, where y^a are the outputs of the robot (computed via kinematics) and y^d_α are the outputs of the human as represented by the ECHF. As the dynamics of the robot model are highly nonlinear, the natural choice of control method for this system is feedback linearization [34].

4.1. Parameterization of time

Autonomous control has several advantages for the control of bipedal robots (see [35]). With this consideration, we introduce a state-based parameterization of time in our system; this is a common practice in [10, 12]. As shown in Section 2.4, analysis of human data reveals that the linearized forward position of the hip δp_{hip} evolves in an approximately linear manner with respect to time, that is, $\delta p_{hip}(t, v_{hip}) \approx v_{hip} t$. Taking advantage of this observation, the following parameterization of time is formed:

$$\tau(q) = \frac{\delta p^R_{hip}(q) - \delta p^R_{hip}(q^+)}{v_{hip}}, \tag{13}$$

where $\delta p^R_{hip}(q^+)$ is the linearized forward position of the hip at the beginning of the current step.

4.2. Controller specification

With the parameterization of time in place, the control law can be defined explicitly with the ECHF discussed in Section 2. Particularly, we define the (relative degree 2) actual outputs of the robot to be the output functions considered in Section 2 and the desired outputs to be the outputs of the human as represented by the ECHF but with parameterized time $\tau(q)$:

$$y^a_2(q) = \begin{bmatrix} \theta_{hip} \\ \theta_{sk} \\ \theta_{nsk} \end{bmatrix}, \; y^d_{2,\alpha}(q) = \begin{bmatrix} \theta^d_{hip}(\tau(q), \alpha_{hip}) \\ \theta^d_{sk}(\tau(q), \alpha_{sk}) \\ \theta^d_{nsk}(\tau(q), \alpha_{nsk}) \end{bmatrix}. \tag{14}$$

Similarly, with the goal of controlling the velocity of the robot, we define the relative degree 1 outputs to be the velocity of the hip and the desired velocity of the hip:

$$y^a_1(q, \dot{q}) = d\delta p_{hip}(q)\dot{q}, \qquad y^d_{1,\alpha} = v_{hip}. \tag{15}$$

The goal is for the outputs of the robot to agree with the outputs of the human, motivating the final form of the human-inspired outputs to be used in feedback linearization:

$$y_\alpha(q, \dot{q}) = \begin{bmatrix} y_{1,\alpha}(q, \dot{q}) \\ y_{2,\alpha}(q) \end{bmatrix} = \begin{bmatrix} y^a_1(q, \dot{q}) - v_{hip} \\ y^a_2(q) - y^d_{2,\alpha}(q) \end{bmatrix}. \tag{16}$$

Therefore, the feedback linearization controller, $u_\alpha(q, \dot{q})$, can now be stated as follows:

$$u_\alpha(q, \dot{q}) = -\mathcal{A}^{-1}_\alpha(q, \dot{q}) \left(\begin{bmatrix} 0 \\ L_f L_f y_{2,\alpha}(q, \dot{q}) \end{bmatrix} + \begin{bmatrix} L_f y_{1,\alpha}(q, \dot{q}) \\ 2\varepsilon L_f y_{2,\alpha}(q, \dot{q}) \end{bmatrix} + \begin{bmatrix} \varepsilon y_{1,\alpha}(q, \dot{q}) \\ \varepsilon^2 y_{2,\alpha}(q) \end{bmatrix} \right), \tag{17}$$

with control gain ε and decoupling matrix $\mathcal{A}_\alpha(q, \dot{q})$ given by

$$\mathcal{A}_\alpha(q, \dot{q}) = \begin{bmatrix} L_g y_{1,\alpha}(q, \dot{q}) \\ L_g L_f y_{2,\alpha}(q, \dot{q}) \end{bmatrix}.$$

Because of the criterion that the outputs should be mutually exclusive [18], the decoupling matrix is guaranteed to be nonsingular. It follows that for a control gain $\varepsilon > 0$, the control law u_α renders

DOI: 10.1002/oca

the outputs exponentially stable [34]. That is, the outputs of the robot converge to the ECHF exponentially. Note that because the parameters α are so important and change for each motion primitive, we explicitly define the controller u_α and desired output functions y_α^d corresponding to α. The goal of Section 6 will be to determine the parameters, α, of this control law to achieve different walking behaviors based upon the human data.

5. HYBRID AND META-HYBRID SYSTEMS

In this section, it is shown that primary modes of bipedal locomotion—such as walking, standing, and traversing stairways—can each be represented by a unique hybrid control system. However, control of functional bipedal robots requires dominion over *multiple* primary modes of locomotion. Therefore, to develop a functional locomotion control scheme, one must introduce auxiliary hybrid systems, which evolve the state of the robot during transitions between primary modes. To this end, we propose the concept of a meta-hybrid system, which consists of both primary and auxiliary hybrid systems formally merged together in a way that allows for the motion planning through both motion primitives and motion transitions.

5.1. Hybrid system for the biped

Given the Lagrangian and impact dynamics of the robot model in Section 3, a natural choice of mathematical representation for this model is a hybrid system [18], which exhibits both continuous and discrete dynamics. Formally, we begin by writing the hybrid control system for the robot as

$$\mathscr{HC}_h^R = (\mathcal{D}_h^R, \mathcal{S}_h^R, \Delta^R, f^R, g^R, U^R), \tag{18}$$

which depends on a unilateral constraint function, h, representing the *terrain* of the hybrid system. The superscript R denotes that the following notations are for the robot in this paper particularly. Specifically, h is the height of the nonstance foot above the walking surface, for example, a staircase or level ground, and h characterizes the allowable configuration, that is, the domain. With both feet on flat ground, the stationary behavior domain is defined as follows:

$$\mathcal{D}_{h_s}^R = \left\{ (q, \dot{q}) \in T\mathcal{Q} : h_s(q) = 0 \text{ and } \frac{\partial h_s(q)}{\partial q}\dot{q} = 0 \right\}. \tag{19}$$

Similarly, the domain of mobile behaviors can be stated as follows:

$$\mathcal{D}_{h_m}^R = \{ (q, \dot{q}) \in T\mathcal{Q} : h_m(q) \geq 0 \}. \tag{20}$$

The guard is the boundary of the domain with the additional assumption that the unilateral constraint is decreasing, as stated as follows:

$$\mathcal{S}_h^R = \left\{ (q, \dot{q}) \in T\mathcal{Q} : h(q) = 0 \text{ and } \frac{\partial h(q)}{\partial q}\,\dot{q} < 0 \right\}. \tag{21}$$

The remaining elements are specified by the dynamics of the robot; that is, they are intrinsic to the model and consistent for all hybrid system representations of the robot, yet they are independent of the terrain. These elements are given by

- Δ^R is the reset map, corresponding to the *impact equations* as defined in (12),
- $U^R = \mathbb{R}^4$, as we assume full control authority.

Applying the human-inspired feedback control law $u(q, \dot{q})$ as defined in (17), we have the hybrid system as

$$\mathscr{H}_{(h,\alpha)}^R = (\mathcal{D}_h^R, \mathcal{S}_h^R, \Delta^R, f_\alpha^R), \tag{22}$$

with $f_\alpha^R(q, \dot{q}) = f^R(q, \dot{q}) + g^R(q)u_\alpha(q, \dot{q})$.

DOI: 10.1002/oca

Note that, as stated in Section 3.1, we have different (f^R, g^R) with respect to the domains, that is, the types of motion primitive. Therefore, with different domains and (f^R, g^R), we define the different types of hybrid control system as $\mathscr{H}^{R,i}_{(h,\alpha)}$ with $i = s$ or m corresponding to the stationary motion primitive or mobile motion primitives. The more detailed explanation about the notations can be referred to Table III and IV.

For each type of hybrid system, we have made the dependence of f^R_α on the parameters $\alpha \in \mathbb{R}^{22}$ of the human walking functions explicitly (note that f^R_α also depends on the control gain ϵ, but because the same gain will be used in all cases for the robot, it is not explicitly stated). The end result of the modeling process is that two different types of hybrid system are defined based on the types of motion primitive. Specifically, for each type of motion, a hybrid system $\mathscr{H}^{R,i}_{(h,\alpha)}$ that depends on the type of behavior (through $i = s$ or m), the terrain it is walking on (through h), and the parameters of the human-inspired control α has been defined.

Table III. Definition of primary symbols.

θ_{sf}	Stance ankle angle	$\mathcal{D}$	Domain of hybrid system
θ_{hip}	Nonstance hip angle	S	Switching surface of hybrid system
θ_{sk}	Stance knee angle	(f, g)	Affine control system of hybrid system
θ_{nsk}	Nonstance knee angle	U	Set of admissible control
α	Parameter vector	$\mathcal{X}$	State space
q	Body coordinates of the robot	P	Poincaré map
δp_{hip}	Linearized forward hip position	G	Poincaré section
v_{hip}	Desired forward velocity of the hip	Γ	Directed graph
$y_H(t)$	Extended canonical human function	V	Set of vertices
L	Lagrangian equation	E	Set of edges
A_q	Holonomic constraints matrix	FZ	Full zero dynamics surface
B	Torque distribution matrix	PZ	Partial zero dynamics surface
u	Feedback controller	FHZD	Full hybrid zero dynamics surface
D	Inertial matrix	PHZD	Partial hybrid zero dynamics surface
C	Coriolis matrix	$T\mathcal{Q}$	Tangent space of the configuration space $\mathcal{Q}$
$\mathcal{Q}$	Configuration space	$\mathscr{M}$	Collection of motion primitives
τ_q	Parameterized time w.r.t q	$\mathscr{T}$	Collection of motion transitions
$y_1(q, \dot{q})$	Output of relative degree one	$\mathscr{M}\mathscr{H}$	Meta-hybrid system
$y_2(q)$	Outputs of relative degree 2	$\mathscr{H}\mathscr{C}$	Hybrid control system
$y(q, \dot{q})$	Grouped outputs with different relative degrees	$\mathscr{H}$	Hybrid system
Δ_q	State relabeling matrix	$(\vartheta(\alpha), \dot{\vartheta}(\alpha))$	Point on the intersection of the FHZD surface and the guard
$\Delta_{\dot{q}}$	Velocity relabeling procedure	$(q^*_{\epsilon,v}, \dot{q}^*_{\epsilon,v})$	Fixed point of specified motion primitive v with control gain ϵ
ϵ	Controller gain	$\mathcal{A}(q, \dot{q})$	Decoupling matrix

Table IV. Definition of superscript and subscript symbols.

Superscript symbols		Subscript symbols	
N^R	Notation for robot	N_v	Notation for motion primitives. $v \in \{ss, fg, us, ds\}$
N^a	Notation for actual outputs	N_e	Notation for motion transitions. $e \in \{(ss, fg), (fg, ss), (fg, us), (us, fg), (fg, ds), (ds, fg)\}$
N^d	Notation for desired outputs	N_α	Notation w.r.t specified α
N^H	Notation for human data or outputs	N_h	Notation w.r.t specified guard h
N^*	Optimized parameter	$\mathrm{N}_{tar(e)}$	Target motion primitive for motion transition e
$\mathrm{N}^{f\to u}$	Transition from flat ground to upstairs (other similar notations have similar meaning)	$\mathrm{N}_{sor(e)}$	Source motion primitive for motion transition e
N^m	Mobile related locomotion	N^s	stationary related locomotion

N stands for any primary notation that appeared in Table III. For example, α^*_e stands for the optimized parameter of motion transition e.

DOI: 10.1002/oca

5.2. Meta-hybrid systems

A meta-hybrid system is a hybrid system of hybrid systems, which contains multiple locomotion behaviors and transitions between these behaviors.

Definition 1
A *meta-hybrid system* is a tuple,

$$\mathscr{MH} = (\Gamma, \mathscr{M}, \mathscr{T}),$$

where

- $\Gamma = (V, E)$ is a directed graph, with V as a set of vertices, or nodes, and $E \subset Q \times Q$ a set of edges; for $e = (q, q') \in E$, denote the source of e by $\mathrm{sor}(e) = q$ and the target of e by $\mathrm{tar}(e) = q'$.
- $\{\mathscr{M}_v\}_{v \in V}$ is a collection of *motion primitives*, each represented by a hybrid system:

$$\mathscr{M}_v = (\mathcal{D}_v, \mathcal{S}_v, \Delta_v, f_v).$$

- $\{\mathscr{T}_e\}_{e \in E}$ is a collection of *motion transitions*, represented by hybrid systems of the form:

$$\mathscr{T}_e = (\mathcal{D}_{\mathrm{tar}(e)}, \mathcal{S}_{\mathrm{tar}(e)}, \Delta_{\mathrm{tar}(e)}, f_e).$$

  That is, $\mathscr{T}_e$ has the same domain, guard, and reset map as $\mathscr{M}_{\mathrm{tar}(e)}$ but has a different vector field f_e.

5.2.1. Hybrid period orbits and the Poincaré map. In order to establish the stability of k-periodic orbits, we will use the standard technique of studying the corresponding Poincaré map. In particular, taking G to be the Poincaré section, one obtains the Poincaré map, $P : G \to G$, which is a partial map defined by

$$P(z) = c(\tau(z)),$$

where $c(t)$ is the solution to $\dot{x} = f(x)$ with $c(0) = R(z)$ and $\tau(z)$ is the *time-to-impact* function. In particular, if z^* is a k- with defining z^* as the k-fixed point of P (under suitable assumptions on z^*, G, and the transversally of $\mathcal{O}$ and G) a k-periodic orbit $\mathcal{O}$ with $z^* \in \mathcal{O}$ is locally exponentially stable if and only if P^k is locally exponentially stable (as a discrete-time dynamical system, $z_{i+1} = P(z_i)$)(the detailed definition can also be seen in [19]). Although it is not possible to explicitly compute the Poincaré map, one can compute a numerical approximation of this map through simulation and thereby test its stability numerically. This gives a concrete method for practically testing the stability of periodic orbits.

In this paper, we consider a Poincaré map for hybrid systems (e.g., a meta-hybrid system) that are no longer 'simple'—meaning that they exhibit multidomain, that is, more than one type of impact will happen. The stability of a hybrid system that undergoes sequences of different domains has been discussed in detail in [36]. Particularly, a periodic orbit can be constructed transversally; therefore, a nontrivial Poincaré map can be computed explicitly to numerically prove the stability of a multidomain hybrid system. Here, the robot will evolve through three motion primitives and two motion transitions, which will incur five impacts for one periodic orbit. Numerical approximations of the eigenvalues of the Poincaré map for the meta-hybrid system are obtained by simulating the system, from one motion primitive, through a motion transition, to the next motion primitive. The meta-hybrid system is deemed stable if for every motion primitive–motion transition–motion primitive cycle, the eigenvalues have a magnitude less than unity.

6. MOTION PRIMITIVES AND TRANSITIONS

In this section, we will explicitly construct a meta-hybrid system for a bipedal robot, with the motion primitives and transitions between these behaviors. Following this construction, the execution of this meta-hybrid system will be introduced. The resulting behavior displayed by the robot,

DOI: 10.1002/oca

while performing these transitions and motion primitives, will be shown via results from simulation. Formally, the goal of this section is to construct a meta-hybrid system for the bipedal robot:

$$\mathscr{MH}^R = (\Gamma^R, \mathscr{M}^R, \mathscr{T}^R).$$

With the four motion primitives, standing still on flat ground ss, walking on flat ground fg, upstairs us, and downstairs ds, we have the directed graph $\Gamma^R = (V^R, E^R)$, where

$$\begin{aligned} V^R &= \{ss, fg, us, ds\}, \\ E^R &= \{(ss, fg), (fg, stp), (fg, us), (us, fg), (fg, ds), (ds, fg)\}. \end{aligned}$$

Note that the transitions between standing still on flat ground to going upstairs or downstairs and the transitions between going upstairs and downstairs are not considered in this work for the sake of simplicity, but the methods outlined in this paper could still be applied. The total graph Γ^R can be seen in Figure 7. The remainder of this section will be devoted to constructing the motion primitives and motion transitions.

6.1. Motion primitives

Motion primitives are the core modes of locomotion of this study; this section discusses the development of controllers for motion primitives and the simulations resulting from the application of these controllers to the robot model.

6.1.1. Motion primitive collection. Using the concepts developed throughout this paper, we can now construct mathematical representations of a bipedal robot conducting each of the four different motion primitives of interest. In particular, we can model the robot in different domains as follows:

- *standing still on flat ground:* $\mathscr{H}^{R,s}_{(h_{ss},\alpha_{ss})}$, where $h_{ss}(q) = 0$,
- *walking on flat ground:* $\mathscr{H}^{R,m}_{(h_{fg},\alpha_{fg})}$, where $h_{fg}(q) = z_{nsf}(q)$,
- *walking upstairs:* $\mathscr{H}^{R,m}_{(h_{us},\alpha_{us})}$, where $h_{us}(q) = z_{nsf}(q) - z_{stair}$,
- *walking downstairs:* $\mathscr{H}^{R,m}_{(h_{ds},\alpha_{ds})}$, where $h_{ds}(q) = z_{nsf}(q) + z_{stair}$.

The superscript s of $\mathscr{H}^{R,s}_{(h_{ss},\alpha_{ss})}$ corresponds to the stationary motion primitive with the affine control system defined by (10) in which the holonomic constraints are enforced and the domain is defined by (19). Similarly, the mobile motion primitives are denoted with superscript m with the control

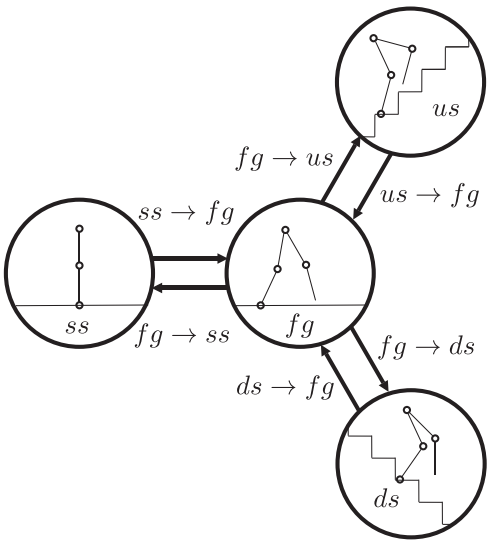

Figure 7. Meta-system representation for the four motion primitives in consideration.

DOI: 10.1002/oca

system defined by (11) and the domain defined by (20). To effect these behaviors on the robot, it is necessary to design controllers for each motion primitive, that is, determine the control parameters α_v, $v \in V^R$, which will result in stable walking for the robot in each domain.

6.1.2. Controller development. Because of the differences between the two groups of motion primitives, we introduce two different methods of obtaining the control parameters α_v, $v \in V^R$.

Stationary motion primitive. For the stand still motion primitive, holonomic constraints and Lagrange multipliers are introduced to ensure that both feet are pinned to the ground while the angles and the velocities of the system are driven to zero. A time-based tracking controller, therefore, is constructed for the stationary motion primitive.

Mobile motion primitives. The goal of this section is to discuss the main result of this paper; that is, starting from human data directly, through an optimization algorithm, which is subject to specific constraints, we obtain control parameters α_v, $v \in V^R$ for all three mobile motion primitives. These control parameters guarantee stable walking while simultaneously achieving a high degree correlation fit to the human data. This methodology has been discussed in [18] for the case of flat-ground walking. Here, we extend the methodology to all the three mobile motion primitives. We also show that, with reasonable modifications to this methodology, we can achieve remarkable results for motion transitions—a topic that will be discussed in later sections.

6.1.3. Partial hybrid zero dynamics. As discussed in Section 4, the goal of the control law u_α (17) is to drive the human-inspired output $y_\alpha(q, \dot{q}) \to 0$ exponentially at a rate of ϵ. Therefore, for the *continuous* dynamics, the controller renders the *full zero dynamics surface*:

$$\mathbf{FZ}_\alpha = \{(q, \dot{q}) \in T\mathcal{Q}_R : y_\alpha(q, \dot{q}) = \mathbf{0},\ L_{f_R} y_{2,\alpha}(q) = \mathbf{0}\}. \tag{23}$$

While this surface is invariant for continuous dynamics, however, this is not the case for discrete dynamics. In particular, the discrete impacts in the system cause the state to be 'thrown' off of the zero dynamics surface. Therefore, a hybrid system has *full hybrid zero dynamics* if the zero dynamics are invariant through impact: $\Delta^R(S^R \cap \mathbf{FZ}_\alpha) \subset \mathbf{FZ}_\alpha$ [18].

While the realization of FHZD renders many 'nice' properties for the system, it is quite difficult in the case of bipedal robotic walking because it would force the highly nonlinear hybrid system to evolve on a 1D manifold. Therefore, we seek to enforce zero dynamics only for the relative degree 2 outputs. We refer to this as the *partial zero dynamics surface*, given by

$$\mathbf{PZ}_\alpha = \{(q, \dot{q}) \in T\mathcal{Q}_R : y_{2,\alpha}(q) = \mathbf{0},\ L_{f_R} y_{2,\alpha}(q) = \mathbf{0}\}. \tag{24}$$

Particularly, we can define the PHZD as $\Delta^R(S^R \cap \mathbf{FZ}_\alpha) \subset \mathbf{PZ}_\alpha$. The consideration of this modification is that PHZD allows some 'freedom' in the movement of the system to account for differences between the robot model and human. Moreover, because the only output that is not included in the partial zero dynamics surface is the output that forces the forward hip velocity to be constant, enforcing PHZD simply means that we allow the velocity of the hip to compensate for the shocks in the system due to impact. After constraining the system on the PHZD surface invariantly through impact, we will achieve a system evolving with a 2D zero dynamics manifold that is determined by the parameters α only. Note that the PHZD surface is consistent for all three mobile motion primitives; thus, the conclusion obtained in [19] for walking on flat ground also applies for the remaining two motion primitives.

6.1.4. Human-inspired optimization. With the PHZD in mind, the goal to develop the controller becomes to find parameters α_v^* that solve the following constrained optimization problem:

$$\alpha = \underset{\alpha_v \in \mathbb{R}^{22}}{\operatorname{argmin}}\ \mathrm{Cost}_{\mathrm{HD}}(\alpha_v) \tag{25}$$

$$\text{s.t} \quad \Delta^R(S^R_{h_v} \cap \mathbf{FZ}_{\alpha_v}) \subset \mathbf{PZ}_{\alpha_v}, \tag{PHZD}$$

DOI: 10.1002/oca

with $\mathrm{Cost}_{\mathrm{HD}}$ being the same as that in (6) and $v \in \{fg, us, ds\}$. This is simply the optimization problem in (6) that is used to determine the parameters of the ECHF to give the best fit of the human walking functions to the human output data of three motion primitives but subject to constraints that ensure PHZD. Note that $S^R_{h_v}$ are different for different motion primitives. This method can be applied to all three mobile motion primitives; the only difference is the height above the walking surface h_v, that is, the guard.

In order to solve (25) explicitly, we restate the PHZD constraints with applying the inverse kinematics methodology discussed in [18] in such a way that it can be practically solved. Specifically, because of the formula of the outputs we choose (all outputs are linear) and the way we parameterize the time, a point $(\vartheta_v(\alpha_v), \dot{\vartheta}_v(\alpha_v)) \in \mathbf{FZ}_{\alpha_v} \cap S^R_{h_v}$ on the intersection of the full zero dynamics surface and the switching surface can be explicitly computed in terms of the parameters α_v (detail derivation can be seen in [18]). Therefore, with the notation of partial zero dynamics surface and the point $(\vartheta_v(\alpha_v), \dot{\vartheta}_v(\alpha_v))$, we formally redefine PHZD as the following *human-inspired optimization problem* theorem:

Theorem 1
The parameters α^*_v solving the constrained optimization problem

$$\alpha = \underset{\alpha_v \in \mathbb{R}^{21}}{\operatorname{argmin}} \ \mathrm{Cost}_{\mathrm{HD}}(\alpha_v) \tag{26}$$

$$\text{s.t} \quad y_{2,\alpha}(\vartheta_v(\alpha_v)) = \mathbf{0} \tag{C1}$$

$$dy_{2,\alpha}(\Delta_\theta \vartheta_v(\alpha_v))\Delta_{\dot{\theta}}(\vartheta_v(\alpha_v))\dot{\vartheta}_v(\alpha_v) = \mathbf{0} \tag{C2}$$

$$dh^R_v(\vartheta_v(\alpha_v))\dot{\vartheta}_v(\alpha_v) < 0 \tag{C3}$$

yield hybrid zero dynamics: $\Delta^R(S^R_{h_v} \cap \mathbf{FZ}_{\alpha^*_v}) \subset \mathbf{PZ}_{\alpha^*_v}$. Furthermore, if

$$\tau(\vartheta_v(\alpha^*_v)) = \frac{\delta p^R_{hip}(\vartheta_v(\alpha^*_v)) - \delta p^R_{hip}(\Delta_q \vartheta^*_v)(\alpha^*_V)}{v_{hip,v}} > 0,$$

then there exists a constant $\bar{\epsilon} > 0$ such that for all $\epsilon > \bar{\epsilon}$, the hybrid system $\mathscr{H}^{R,m}_{(h_v,\alpha^*_v)}$ has an exponentially stable periodic orbit. Moreover, the fixed point of this periodic orbit, $(q^*_{\epsilon,v}, \dot{q}^*_{\epsilon,v})$, satisfies the property that

$$\lim_{\epsilon \to \infty} (q^*_{\epsilon,v}, \dot{q}^*_{\epsilon,v}) = (\vartheta_v(\alpha^*_v), \dot{\vartheta}_v(\alpha^*_v)). \tag{27}$$

This theorem follows from a combination of Theorem 1 in [18] and Theorem 2 in [19] but is extended to the case of different motion primitives. The proof of this theorem is also similar to the proof in those two papers; because this proof would require the introduction of numerous constructions that are not necessary to the rest of the results given in this paper, we will not state it in explicit detail. The only difference is that for different motion primitives, we have different guards $h_v(q)$—which renders the proof, for the most part, unchanged. The proof of the first part of Theorem 1 is the same as in [18] because PHZD is invariant corresponding to the height guard. For the proof of the second part, it is similar to the proof of Theorem 2 in [19] but with a constant shift in the Poincaré map for different motion primitives (different guards); however, these shifts do not affect the proof of the existence of the fixed point $(\vartheta_v(\alpha^*_v), \dot{\vartheta}_v(\alpha^*_v))$. Note that Theorem 1 does not guarantee the convergence to the fixed point but ensures the existence of the fixed point if the optimization problem subject to the PHZD constraints can be solved. It is these special constraints that guarantee stable walking that are the highlights of this optimization paper. Again, as we know that these constraints are highly nonlinear, it is difficult (if not impossible) to locate or to identify

DOI: 10.1002/oca

the global minimum. However, we argue that with sufficient small feasibility, we can conclude that a good solution that guarantees stable walking with PHZD will be found. Feasibility, one of the outputs of MATLAB built-in function *fmincon*, denotes the maximum constraint violation.

Now, we can restate the main result of this paper; starting from the human data, through the inverse kinematics and the parameters obtained from optimization problem (26), we can determine the fixed points $(\vartheta_v(\alpha_v^*), \dot{\vartheta}_v(\alpha_v^*))$, where $v \in \{fg, us, ds\}$, to the stable hybrid periodic orbits of all three mobile motion primitives. Because the cost function of the optimization problem only depends

(a) Walking on flat ground.

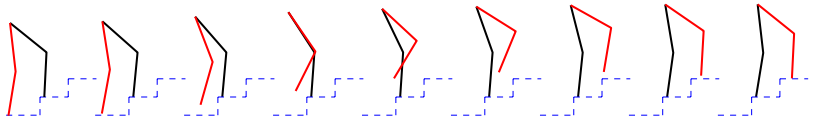

(b) Walking upstairs.

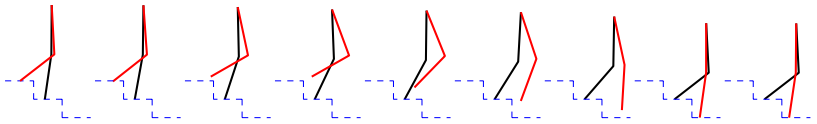

(c) Walking downstairs.

Figure 8. Snapshots from robotic locomotion simulations exhibiting the three motion primitives.

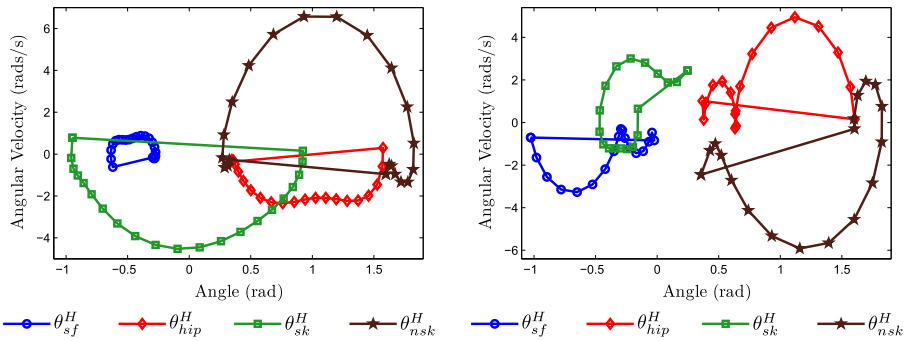

(a) Periodic orbit for $\mathscr{M}_{as}$. (b) Periodic orbit for $\mathscr{M}_{ds}$.

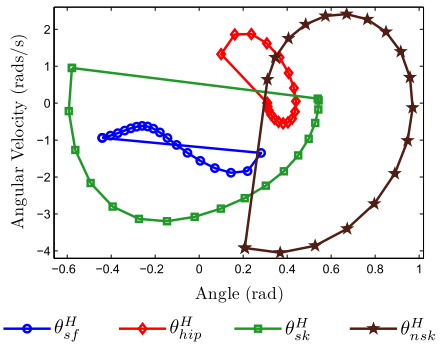

(c) Periodic orbit for $\mathscr{M}_{fg}$.

Figure 9. Phase portraits for the motion primitives.

DOI: 10.1002/oca

on the human walking data, we reinforce the fact that we can automatically generate a controller, which yields a stable walking gait and the fixed point of its stable hybrid periodic orbit, by only using the human walking data—for all three mobile motion primitives.

6.1.5. Simulation results. Using the results of Theorem 1, which yields the parameters for the human-inspired controller α_v^*, along with a fixed point to the Poincaré map, we obtain stable walking for each motion primitive. Note that the feasibility of each case is less than $1e-10$. The resulting locomotion gaits from simulation are given in Figure 8; these figures show the evolution of the robot during the single support phase of the gait, each of which qualitatively resembles the corresponding human gait quite well. The video for each motion primitive can be seen in [37]. The phase portraits for each motion primitive simulation are shown in Figure 9. The stability of each phase portrait is numerically verified via numerical approximation of the eigenvalues of the Poincaré map. All maximum eigenvalues are less than 1 as shown in Figure 10, which implies that the corresponding motion primitives are stable. Note that during the review process of this paper, we also achieved bipedal robotic running (with a speed of 2.5 m/s) using the human-inspired optimization with ECHF (see [38]).

Along with stable walking, the simulation results show that the bipedal model considered in this paper has achieved human-like walking for each mobile motion primitive. Table V contains the specific parameters α_v^* obtained through the optimization mentioned earlier. The correlations are all higher than 0.96, which are close to the fitting correlations, and costs from optimization are low. Plots of the human walking functions with these parameters, as compared with the human data, can be seen in Figure 11. From the figure and the table, one can conclude that the bipedal robot considered in this paper, with human-inspired locomotion controller, has achieved qualitatively human-like walking. It is also important to note that the velocities after impact for all motion primitives are below 7 rad/s, which is quite realistic in a physical context.

6.2. *Motion transitions*

This section discusses the development and simulation of motion transitions, which are explicitly built upon the motion primitives obtained in the previous section.

6.2.1. Motion transition collection. We are interested in developing motion primitives based upon the meta-hybrid system graph Γ^R, which gives the allowable transitions between different walking behaviors. Based upon the definition of a meta-hybrid system (Definition 1), the motion transitions must satisfy very specific conditions with regard to the motion primitives. Therefore, the specific motion transition hybrid systems we are interested in must have the form

- *standing still to walking on flat ground:* $\mathscr{H}^{R,s}_{(h_{fg},\alpha_{(ss,fg)})}$, where $h_{fg}(q) = z_{nsf}(q)$;
- *walking on flat ground to stand still:* $\mathscr{H}^{R,s}_{(h_{ss},\alpha_{(fg,ss)})}$, where $h_{ss}(q) = 0$;
- *walking on flat ground to upstairs:* $\mathscr{H}^{R,m}_{(h_{us},\alpha_{(fg,us)})}$, where $h_{us}(q) = z_{nsf}(q) - z_{stair}$;
- *walking upstairs to flat ground:* $\mathscr{H}^{R,m}_{(h_{fg},\alpha_{(us,fg)})}$, where $h_{fg}(q) = z_{nsf}(q)$;
- *walking on flat ground to downstairs:* $\mathscr{H}^{R,m}_{(h_{ds},\alpha_{(fg,ds)})}$, where $h_{ds}(q) = z_{nsf}(q) + z_{stair}$;
- *walking downstairs to flat ground:* $\mathscr{H}^{R,m}_{(h_{fg},\alpha_{(ds,fg)})}$, where $h_{fg}(q) = z_{nsf}(q)$.

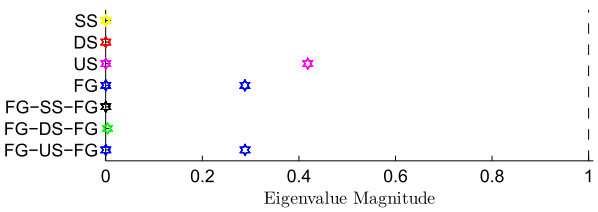

Figure 10. Eigenvalues of motions.

DOI: 10.1002/oca

Table V. Optimized parameter values and cost for human functions.

$y_1^a = a_1 t, \quad y_2^a = y_H(t)$ given in (4)									
Function	a_1	a_2	a_3	a_4	a_5	a_6	a_7	Correlation	Cost
δp_{hip}^{fg}	0.925	0	0	0	0	0	0	0.9991	*
θ_{hip}^{fg}	−1.941	0.320	5.865	−0.109	0	0	0.267	0.9958	*
θ_{sk}^{fg}	4.852	−0.223	12.01	0.125	0	0	0.323	0.9787	*
θ_{nsk}^{fg}	−0.617	−0.330	9.381	0.209	0	0	0.649	0.9948	1.179
δp_{hip}^{us}	0.623	0	0	0	0	0	0	0.9985	*
θ_{hip}^{us}	3.790	1.428	5.942	1.090	0.025	20.87	−0.648	0.9993	*
θ_{sk}^{us}	6.409	0.772	2.059	3.175	0.007	9.191	0.203	0.9956	*
θ_{nsk}^{us}	−3.037	0.292	2.842	0.200	−0.267	12.01	0.274	0.9987	0.868
δp_{hip}^{ds}	0.535	0	0	0	0	0	0	0.9981	*
θ_{hip}^{ds}	3.658	−1.926	0.246	−7.356	0.320	4.766	1.541	0.9656	*
θ_{sk}^{ds}	0.296	−10.727	0.484	−5.320	−0.102	17.57	10.98	0.9830	*
θ_{nsk}^{ds}	6.960	−0.547	11.31	−0.870	0.586	7.978	0.964	0.9956	2.817
$\delta p_{hip}^{f\to u}$	0.760	0	0	0	0	0	0	0.9993	*
$\theta_{hip}^{f\to u}$	−3.014	0.196	4.825	−0.126	0.284	11.12	0.106	0.9984	*
$\theta_{sk}^{f\to u}$	0.841	−0.148	6.676	1.062	0.082	6.822	0.167	0.9091	*
$\theta_{nsk}^{f\to u}$	1.367	−0.602	10.02	0.069	0.009	15.93	0.911	0.9991	3.113
$\delta p_{hip}^{u\to f}$	0.774	0	0	0	0	0	0	0.9981	*
$\theta_{hip}^{u\to f}$	0.854	0.828	4.000	−0.410	0.095	10.01	−0.118	0.9999	*
$\theta_{sk}^{u\to f}$	2.455	0.498	2.063	−1.113	0.011	24.18	0.474	0.9822	*
$\theta_{nsk}^{u\to f}$	0.852	−0.163	6.802	1.067	−0.000	6.855	0.462	0.9931	2.000
$\delta p_{hip}^{f\to d}$	0.730	0	0	0	0	0	0	0.9990	*
$\theta_{hip}^{f\to d}$	−1.568	0.138	4.988	−0.212	0.216	12.27	0.232	0.9494	*
$\theta_{sk}^{f\to d}$	0.239	6.709	0.235	15.74	0.126	13.72	−6.735	0.9382	*
$\theta_{nsk}^{f\to d}$	0.587	6.138	0.482	9.738	−0.257	16.32	−5.46	0.4249	10.22
$\delta p_{hip}^{d\to f}$	0.730	0	0	0	0	0	0	0.9996	*
$\theta_{hip}^{d\to f}$	−0.717	0.731	4.147	1.574	0.977	14.05	−1.772	0.9302	*
$\theta_{sk}^{d\to f}$	−0.060	−9.575	0.273	4.584	0.062	17.48	9.661	0.2506	*
$\theta_{nsk}^{d\to f}$	0.560	2.269	6.766	2.642	−1.386	6.518	0.949	0.9396	11.66

Note that, the cost is the combination cost of all the four outputs. The asterisk indicates that the cost of each individual output is not available here but will be sent upon request.

Because we have two types of motion primitives, the methodology to determine the control parameters α_e^*, $e \in E$ corresponding to different transitions will be different. Therefore, we separate the six motion transitions into two groups: the first group contains two motion transitions related to the stand still motion primitive, which are $\mathscr{H}^{R,s}_{(h_{fg},\alpha_{(ss,fg)})}$ and $\mathscr{H}^{R,s}_{(h_{ss},\alpha_{(fg,ss)})}$; the remaining four motion transitions belong to the second group. We name the first group as 'stationary related motion transitions' and the second group as 'mobile related motion transitions'. In the following section, we discuss the optimization problems through which the motion transitions are obtained.

6.2.2. Controller development. Motion transitions connect two different motion primitives. Therefore, we have to take both the source and target motion primitives into consideration while we are constructing optimizations for motion transitions.

Stationary related motion transitions. To determine the parameters α_e^*, $e \in E$, of the stationary related motion transitions, we use the fixed points corresponding to motion primitives of standing

DOI: 10.1002/oca

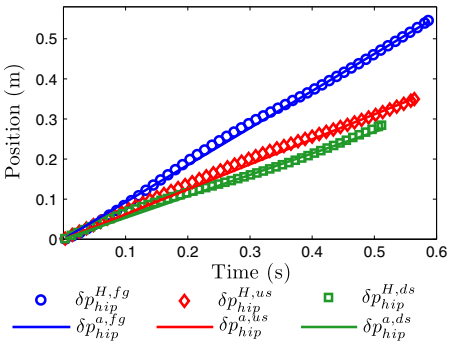

(a) Optimized hip position of mean data

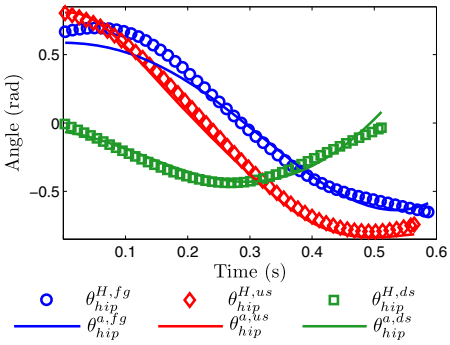

(b) Optimized nonstance hip angle of mean data

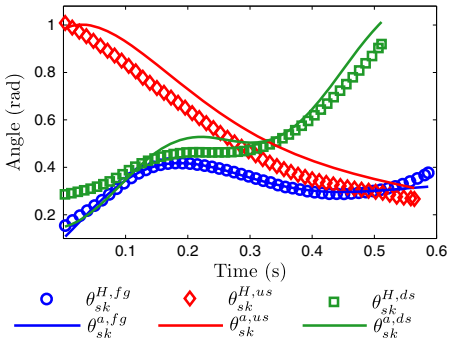

(c) Optimized stance knee angle of mean data

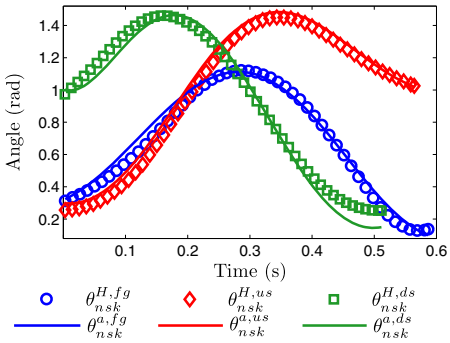

(d) Optimized nonstance knee angle of mean data

Figure 11. Optimized extended canonical human functions with parameters obtained by solving the optimization problem (6) and the corresponding mean human data of three motion primitives.

still on flat ground and flat-ground walking. In particular, $(\vartheta_v(\alpha_v^*), \dot{\vartheta}_v(\alpha_v^*)) \in S^R_{h_v}$, $v \in V^R$ (here, $v \in \{ss, fg\}$) are the fixed points of each motion primitive, which are computed via Theorem 1 in closed form. The second main result of this paper can now be stated: Because we can explicitly compute the fixed points of periodic orbits of all three mobile motion primitives with Theorem 1, we propose that utilizing the fixed points obtained earlier in an optimization problem can also render the parameters of controllers for motion transitions. At a high level, the goal of the motion transition optimization is to generate desired output functions, which effect smooth connections, or 'transitions', between the corresponding source and the target motion primitives. Formally, these objectives can be stated in an optimization problem:

$$\begin{aligned} \alpha_e^* = \underset{\alpha \in \mathbb{R}^{22}}{\operatorname{argmin}} \; & (\|(\vartheta_v(\alpha_e), \dot{\vartheta}_e(\alpha_e)) - (\vartheta_{\text{tar}}(e)(\alpha_{\text{tar}(e)}^*), \dot{\vartheta}_{\text{tar}(e)}(\alpha_{\text{tar}(e)}^*))\|) \\ \text{s.t} \quad & y^d_{2,\alpha_e}(0) - y^d_{2,\alpha^*_{sor(e)}}(0) = 0 \\ & \dot{y}^d_{2,\alpha_e}(0) - \dot{y}^d_{2,\alpha^*_{sor(e)}}(0) = 0, \end{aligned} \tag{28}$$

where, here, $y^d_{2,\alpha_e}(t)$ are the desired relative degree 2 outputs of the robot with parameters α_e; $\alpha^*_{\text{tar}(e)}$ and $\alpha^*_{\text{sor}(e)}$ are the optimized parameters of the target and source motion primitives, $\mathscr{M}^R_{\text{tar}(e)}$ and $\mathscr{M}^R_{\text{sor}(e)}$, respectively. They are obtained explicitly by solving the optimization problem (26), and $(\vartheta_{\text{tar}(e)}(\alpha^*_{\text{tar}(e)}), \dot{\vartheta}_{\text{tar}(e)}(\alpha^*_{\text{tar}(e)}))$ is the fixed point of target motion primitive. Note that, here, $tar(e), sor(e) \in \{ss, fg\}$. $(\vartheta_e(\alpha_e), \dot{\vartheta}_e(\alpha_e))$ is the pre-impact point of the end of the transition, which is the point at the intersection of the full zero dynamics surface of the transition and the guard of the target motion primitive (thus, this point can be computed via the methodology of inverse kinematics). Through the cost function, we enforce the end point of the transition to be as close to

DOI: 10.1002/oca

the fixed point of the target motion primitive as possible, while constraining the transition to start with the fixed point of the source motion primitive. Some augmentation constraints, such as angle limits, have been added to ensure that the transition behavior is as human-like as possible. Solving this optimization renders the parameters α_e^* for the two stationary motion transitions.

Mobile related motion transitions. To generate the parameters α_e^*, $e \in E$, of the mobile related motion transitions, we turn to a different approach. As we have the human data for these four motion transitions, we use the same cost function as in (6) with the constraints corresponding to the target and source motion primitives. The problem can be stated as

$$\begin{aligned}
\alpha_e^* = \underset{\alpha\in\mathbb{R}^{22}}{\operatorname{argmin}}\ & \mathrm{Cost}_{\mathrm{HD}}(\alpha_e) \\
\text{s.t}\quad & y^d_{2,\alpha_e}(0) - y^d_{2,\alpha^*_{sor(e)}}(0) = 0 \\
& \dot{y}^d_{2,\alpha_e}(0) - \dot{y}^d_{2,\alpha^*_{sor(e)}}(0) = 0 \\
& y^d_{2,\alpha_e}(\tau_{\alpha_e}, \alpha^*_{tar(e)}, \alpha^*_{sor(e)}) - y^d_{2,\alpha^*_{tar(e)}}(\tau_{\alpha_e}, \alpha^*_{tar(e)}, \alpha^*_{sor(e)}) = 0 \\
& \dot{y}^d_{2,\alpha_e}(\tau_{\alpha_e}, \alpha^*_{tar(e)}, \alpha^*_{sor(e)}) - \dot{y}^d_{2,\alpha^*_{tar(e)}}(\tau_{\alpha_e}, \alpha^*_{tar(e)}, \alpha^*_{sor(e)}) = 0 \\
& \tau_{\alpha_e}, \alpha^*_{tar(e)}, \alpha^*_{sor(e)} = \frac{\delta p^R_{hip}(\vartheta_{tar(e)}(\alpha^*_{tar(e)})) - \delta p^R_{hip}(\Delta_q \vartheta_{sor(e)}(\alpha^*_{sor(e)}))}{v_{hip,e}},
\end{aligned} \tag{29}$$

where the elements are the same as those in (28) except that $tar(e), sor(e) \in \{fg, us, ds\}$; $\mathrm{Cost}_{\mathrm{HD}}(\alpha_e)$ is the cost given in (6) and $e \in E^R$. Note that $\tau_{\alpha_e}, \alpha^*_{tar(e)}, \alpha^*_{sor(e)}$ is an approximation of the transition time interval, which is computed with the assumption that the hip velocity of the transition behavior is constant—examination of human data for the hip position, given in Figure 5(a), reveals that this assumption is reasonable. $\delta p^R_{hip}(\vartheta_{tar(e)}(\alpha^*_{tar(e)}))$ and $\delta p^R_{hip}(\Delta_q \vartheta_{sor(e)}(\alpha^*_{sor(e)}))$ are the pre-impact hip position of target motion primitive and the post-impact hip position of source motion primitive, respectively. And $v_{hip,e}$ is the actual hip velocity of the specified motion transition. The optimization here constrains both the start and end points of transitions to be the fixed points of source and target modes, respectively. From a geometric view, we can interpret this process as constructing a topology transformation going smoothly from one convex invariant set to another convex invariant set. By solving this optimization problem, we obtain parameters α_e^* for all four motion transitions.

In this framework, the motion transitions play an important role in the motion planning of the robot, that is, switching between different motion primitives. Rather than switching directly between different motion primitives (ZMP is used in [39], whereas central pattern generator is used [40]), we utilize the motion transition as a 'buffer' to connect the fixed point of each motion primitive to ensure the stability of system while switching. One main advantage of the introduction of motion transitions is that the system can deal with big variation of the terrain with the guarantee of good stability. Another advantage is that the motion transition generates smooth human-like switching process without using high gain and would not generate torque spikes.

This approach is different from funneling work [41], in which the controllable state space is covered with the regions of attraction from many locally stabilizing controllers to ensure robustness of the transitions. Therefore, the motion planning can be considered as switching between different funnels that, for example, can be computed numerically using the method in [42]. Compared with all the pioneering funneling works [41, 43, 44], we focus more on constructing a directed graph consisting nodes (motion primitives) and edges (motion transitions) instead of building funnels. Then, the motion can be planned in the directed graph through switching among the designed nodes via the corresponding edges. Because the motion transitions are optimized in such a way that the fixed point of motion primitives, which are asymptotically stable, can be connected directly and smoothly, the stability of the motion planning can be guaranteed naturally. Particularly, the numerical method of Poincaré map is used to prove the stability of the transition behaviors, which will be discussed later.

DOI: 10.1002/oca

Note that, as in the case of the optimization for PHZD, we only constrain the relative degree 2 outputs. Thus, some 'freedom' is given to the robot to compensate for the differences between the robot and the physical human body. Solving these two optimization problems yields parameters α_e^*, $e \in E^R$; therefore, yields the motion transition hybrid system: $\mathscr{T}_e = \mathscr{H}^{R,i}_{(h_{\text{tar}(e)},\alpha_e^*)}$ with $e \in E^R$ and $i \in \{s, m\}$.

6.2.3. Simulations results. For the mobile related motion transitions, the simulation results show that the robot considered in this paper achieves human-like motion transitions. Table V contains the specific α_e^* obtained through the optimization for each mobile related motion transition. The correlations of transitions related to going upstairs are all higher than 0.98, and the costs are on par with the costs of the motion primitives. For the transitions corresponding to going downstairs, the correlations are still high (higher than 0.93) except for one output. This could be related to the fact that the experimental human data of going downstairs contain a relatively high amount of noise. Plots of the human walking functions with these parameters, as compared with human data, can be seen in Figure 12.

Three simulations were performed in which motion primitives and motion transitions were combined. To construct a Poincaré map, and thus establish a notion of the stability of a meta-system, the biped must start and end in the same mode; therefore, we chose to simulate three locomotion cycles: walking on flat ground to stand still to walking on flat ground (FG-SS-FG), walking on flat ground to walking upstairs to walking on flat ground (FG-US-FG), and walking on flat ground to walking down stairs to walking on flat ground (FG-DS-FG). Numerical approximation yields eigenvalues for all three simulations; the maximum eigenvalue of each is below unity, which implies that all three meta-systems are stable. The phase portraits of these three meta-systems can be seen in Figure 13, from which it can be seen that all velocities after impact for all three meta-systems

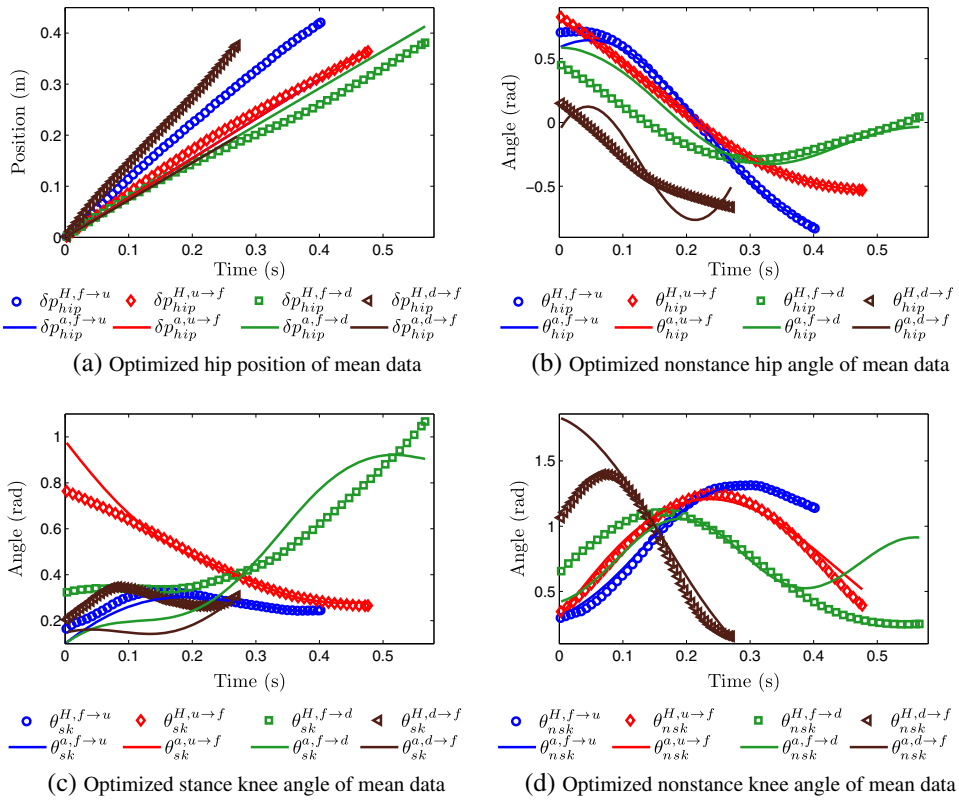

(a) Optimized hip position of mean data

(b) Optimized nonstance hip angle of mean data

(c) Optimized stance knee angle of mean data

(d) Optimized nonstance knee angle of mean data

Figure 12. Optimized extended canonical human functions with parameters obtained by solving the optimization problem (6) and the corresponding mean human data of four motion transitions.

DOI: 10.1002/oca

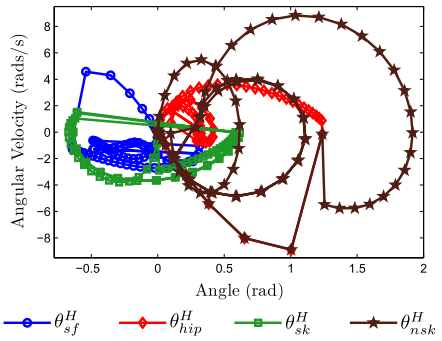

(a) Periodic orbit for $\mathscr{HM}_{\{fg,ss\}}$.

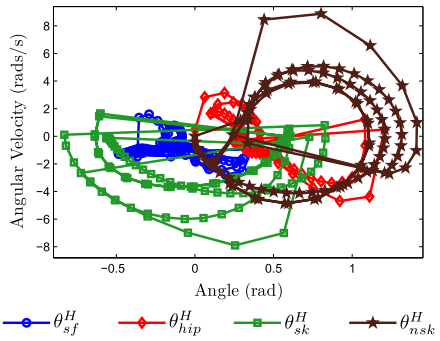

(b) Periodic orbit for $\mathscr{HM}_{\{fg,us\}}$.

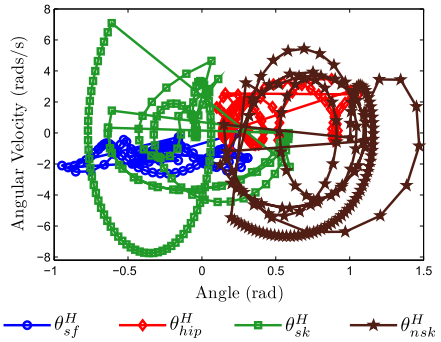

(c) Periodic orbit for $\mathscr{HM}_{\{fg,ds\}}$.

Figure 13. Phase portraits for the combination of motion primitives and motion transitions.

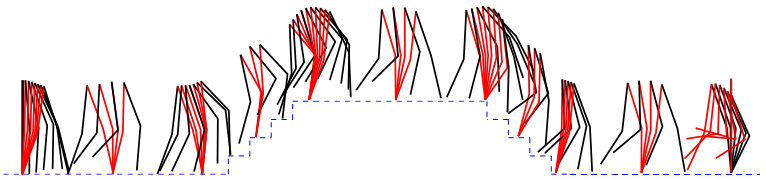

Figure 14. Snapshots from the simulated composition of multiple locomotion modes.

are below 10 rad/s, which is reasonably feasible in practice. Finally, we simulated all four motion primitives together with the six motion transitions; snapshots from the simulation can be seen in Figure 14. And the detailed video that shows the whole process can be seen in [37].

ACKNOWLEDGEMENTS

This research is supported by the NSF grants CNS-0953823 and CNS-1136104, the NHARP award 00512-0184-2009, and the NASA grant NNX11AN06H.

REFERENCES

1. Ambrose RO, Aldridge H, Scott Askew R, Burridge RR, Bluethmann W, Diftler M, Lovchik C, Margruder D, Rehnmark F. NASA Johnson Space Center, Robonaut: NASA's space humanoid. *IEEE Intelligent Systems and their Applications* 2000; **15**:57–63.
2. Matsuno F, Tadokoro S. Rescue robots and systems in Japan. *IEEE International Conference on Robotics and Biomimetics (ROBIO 2004)*, October 2004.
3. Brugger P, Schmiedmayer HB. Simulating prosthetic gait—lessons to learn. *Proceedings in Applied Mathematics and Mechanics* 2003; **3**(1):64–67.

DOI: 10.1002/oca

4. Rai JK, Tewari RP, Chandra D. Hybrid control strategy for robotic leg prosthesis using artificial gait synthesis. *International Journal of Biomechatronics and Biomedical Robotics* 2009; **1**(1):44–50.
5. Kyosuke O, Katsumata M. Analytical study of active prosthetic legs. *Journal of System Design and Dynamics* 2007; **1**(3):548–557.
6. Sakagami Y, Watanabe R, Aoyama C, Matsunaga S, Higaki N, Fujimura K. The intelligent ASIMO: system overview and integration. *IEEE/RSJ International Conference on Intelligent Robots and Systems*, Vol. 3, Lausanne, Switzerland; 2478–2483.
7. McGeer T. Passive dynamic walking. *International Journal of Robotics Research* April 1990; **9**(2):62–82.
8. Collins S, Ruina A, Tedrake R, Wisse M. Efficient bipedal robots based on passive-dynamic walkers. *Science* 2005; **307**:1082–1085.
9. Collins SH, Wisse M, Ruina A. A three-dimensional passive-dynamic walking robot with two legs and knees. *International Journal of Robotics Research* 2001; **20**(2):607–615.
10. Westervelt ER, Grizzle JW, Chevallereau C, Choi JH, Morris B. *Feedback Control of Dynamic Bipedal Robot Locomotion*. CRC Press: Boca Raton, FL, 2007.
11. Rose J, Gamble JG. *Human Walking*. Lippincott Williams & Wilkins: Philadelphia, 2005.
12. Westervelt ER, Grizzle JW, Koditschek DE. Hybrid zero dynamics of planar biped walkers. *IEEE Transactions on Automatic Control* 2003; **48**(1):42–56.
13. Thelen DG, Anderson FC. Using computed muscle control to generate forward dynamic simulations of human walking from experimental data. *Journal of Biomechanics* 2006; **39**(6):1107 –1115.
14. Xiang Y, Chung H-J, Kim JH, Bhatt R, Rahmatalla S. Predictive dynamics an optimization-based novel approach for human motion simulation. *Biomechanical Application* April 2010; **41**(3):465–479.
15. Chevallereau C, Aoustin Y. Optimal reference trajectories for walking and running of a biped robot. *Robotica* 2001; **19**:557–569.
16. Channon PH, Hopkins SH, Pham DT. Derivation of optimal walking motions for a bipedal walking robot. *Robotica* 1992; **10**:165–172.
17. Yadukumar S, Pasupuleti M, Ames A. Human-inspired underactuated bipedal robotic walking with amber on flat-ground, up-slope and uneven terrain. *IEEE/RSJ International Conference on Intelligent Robots and Systems (IROS)*, Algarve, Portugal, 2012; 2478–2483.
18. Ames AD. First steps toward automatically generating bipedal robotic walking from human data. *8th International Workshop on Robotic Motion and Control (RoMoCo 2011)*, Vol. 422, Bukowy Dworek, 2012; 89–116.
19. Ames AD, Cousineau EA, Powell MJ. Dynamically stable bipedal robotic walking with nao via human-inspired hybrid zero dynamics. *Hybrid Systems: Computation and Control*, Beijing, China, 2012; 135–144.
20. Qiu-Bo Z, Song-Hao P, Chao G. Motion planning for humanoid robot based on hybrid evolutionary algorithm. *International Journal of Advanced Robotics Systems* 2010; **7**(3):209–216.
21. Wang Q, Huang Y, Zhu J, Chen B, Wang L. Dynamic walking on uneven terrains with passivity-based bipedal robot. *Informatics in Control Automation and Robotics* 2011; **85**(3):187–199.
22. Yamaguchi J, Takanishi A, Kato I. Development of a biped walking robot adapting to a horizontally uneven surface. *Proceedings of the IEEE/RSJ/GI International Conference on Intelligent Robots and Systems. Advanced Robotic Systems and the Real World (IROS 1994)*, Vol. 2, Munich, Germany, September 1994; 1156–1163.
23. Powell MJ, Zhao H, Ames AD. Motion primitives for human-inspired bipedal robotic locomotion: walking and stair climbing. *2012 IEEE International Conference on Robotics and Automation (ICRA),* May 2012; **543**(549):14–18.
24. Yung-Hui L, Wei-Hsien H. Effects of shoe inserts and heel height on foot pressure, impact force, and perceived comfort during walking. *Applied Ergonomics* 2005; **36**(3):355–362.
25. Frédéric Dierick DR, Massimo P, Detrembleur C. A force measuring treadmill in clinical gait analysis. *Gait & Posture* 2004; **20**(3):299–303.
26. Sinnet RW, Powell MJ, Jiang S, Ames AD. Compass gait revisited: a human data perspective with extensions to three dimensions. *50th IEEE Conference on Decision and Control and European Control Conference*, Orlando, FL, 2011; 682–689.
27. Kramer PA. The effect on energy expenditure of walking on gradients or carrying burdens. *American Journal of Human Biology* 2010; **22**(4):497–507.
28. Yujiang Xiang SR, Arora JS, Abdel-Malek K. Optimization-based dynamic human walking prediction: one step formulation. *International Journal for Numerical Methods in Engineering* 2009; **79**(667–695):291–305.
29. Kolathaya S, Ames A. Achieving bipedal locomotion on rough terrain through human-inspired control. *IEEE International Symposium on Safety, Security, and Rescue Robotics (SSRR 2012)*, College Station, TX, 2012; 1–6.
30. Winter DA. *Biomechanics and Motor Control of Human Movement*, 2nd ed. Wiley-Interscience: New York, 1990.
31. Murray RM, Li Z, Sastry SS. *A Mathematical Introduction to Robotic Manipulation*. CRC Press: Boca Raton, FL, 1994.
32. Hürmüzlü Y, Marghitu DB. Rigid body collions of planar kinematic chains with multiple contact points. *International Journal of Robotics Research* 1994; **13**(1):82–92.
33. Grizzle JW, Abba G, Plestan F. Asymptotically stable walking for biped robots: analysis via systems with impulse effects. *IEEE Transactions on Automatic Control* 2001; **46**(1):51–64.
34. Sastry SS. *Nonlinear Systems: Analysis, Stability and Control*. Springer: New York, 1999.
35. Bekey GA. *Autonomous Robots: From Biological Inspiration to Implementation and Control*. MIT Press: Cambridge, MA, 2005.

DOI: 10.1002/oca

36. Grizzle JW, Chevallereau C, Ames AD, Sinnet RW. 3D bipedal robotic walking: models, feedback control, and open problems. *IFAC Symposium on Nonlinear Control Systems*, Bologna, Italy, September 2010; 505–532.
37. Simulations of human-inspired motion primitives and transitions for bipedal robotic locomotion in diversed terrains, 2012. (Avialable from: http://youtu.be/HTt-y45J7Ro).
38. Zhao H, Yadukumar SN, Ames AD. Bipedal robotic running with partial hybrid zero dynamics and human-inspired optimization. In *IEEE/RSJ International Conference on Intelligent Robots and Systems (IROS 2012)*. IEEE: Vilamoura, Algarve, Portugal, 2012; 1821–1827.
39. Kwon O, Park JH. Asymmetric trajectory generation and impedance control for running of biped robots. *Autonomous Robots* 2008; **26**(1):47–78.
40. Hirukawa H, Kajita S, Harada K, Hattori S, Kaneko K, Morisawa M, Nakaoka S, Kanehiro F. A pattern generator of humanoid robots walking on a rough terrain. *IEEE International Conference on Robotics and Automation (ICRA 2007)*, Roma, 2007; 2181–2187.
41. Burridge RR, Rizzi AA, Koditschek DE. Sequential composition of dynamically dexterous robot behaviors. *The International Journal of Robotics Research* 1999; **18**:534–555.
42. Tedrake R, Manchester IR, Tobenkin M, Roberts JW. LQR-trees: feedback motion planning via sums of squares verification. *International Journal of Robotics Research* 2010; **29**(8):1038–1052.
43. Ilchmann A, Ryan E, Trenn S. Tracking control: performance funnels and prescribed transient behaviour. *Systems & Control Letters* 2005; **54**:655–670.
44. Endisch C, Schroder D. Funnel-control in robotics: an introduction. *Control and Automation* 2008:913–9.

DOI: 10.1002/oca